

PAPER

View Article Online
View Journal | View Issue



Cite this: *Environ. Sci.: Nano*, 2020, 7, 2385

Formation and transformation of schwertmannite through direct Fe^{3+} hydrolysis under various geochemical conditions†

Hong Ying,^a Xionghan Feng,^a Mengqiang Zhu,^b Bruno Lanson,^c Fan Liu^a and Xiaoming Wang^a

Schwertmannite formation and transformation, key processes that influence the speciation, mobility, and environmental fate of associated trace elements in acid mine drainage (AMD), were primarily studied through Fe^{2+} oxidation–hydrolysis. Direct Fe^{3+} hydrolysis is another important schwertmannite formation pathway, but the effects of geochemical conditions on the mineralogical properties of schwertmannite formed via such a pathway are poorly known. Here, the formation of schwertmannite through direct Fe^{3+} hydrolysis enforced by heating or adding OH^- and subsequent transformation were systematically examined under various geochemical conditions. Pure schwertmannite is obtained through Fe^{3+} hydrolysis at 25–60 °C for 12 min and subsequent dialysis for 1–15 days, while minor amounts of goethite appear at higher hydrolysis temperatures. A shorter dialysis time and the presence of K^+ or NH_4^+ both slightly increase schwertmannite crystallinity. During Fe^{3+} hydrolysis by adding OH^- , sulfate-bearing ferrihydrite initially forms and then quickly transforms into schwertmannite. In contrast, pre-formed ferrihydrite does not transform into schwertmannite under the same solution conditions, despite sulfate adsorption. With decreasing Fe^{3+} hydrolysis rate, schwertmannite crystallinity slightly increases and its morphology of “network” structure becomes larger and less dense. As to schwertmannite transformation, high temperature, high pH, and the presence of Fe^{2+} favor its transformation to goethite, while a low Fe^{3+} hydrolysis rate and a high Cl^- concentration hinder the transformation. In contrast, the presence of K^+ or high NH_4^+ concentration favors schwertmannite transformation to jarosite with the former occurring more readily. These new insights into schwertmannite formation and transformation are essential for predicting the environmental fates of associated trace elements in AMD environments.

Received 8th March 2020,
Accepted 7th July 2020

DOI: 10.1039/d0en00252f

rsc.li/es-nano

Environmental significance

The formation and transformation of schwertmannite through direct Fe^{3+} hydrolysis have been systematically investigated under various geochemical conditions. Direct Fe^{3+} hydrolysis is an important pathway of schwertmannite formation in AMD-affected areas, with sulfate-incorporated ferrihydrite as an intermediate product. The Fe^{3+} hydrolysis rate significantly influences the crystallinity, morphology, and structural stability of schwertmannite. High temperature, high pH, and the presence of Fe^{2+} favor its transformation into goethite, while high Cl^- concentration hinders this transformation. Moreover, the presence of K^+ or high NH_4^+ concentration favors schwertmannite transformation to jarosite. These results greatly improve our understanding of schwertmannite formation and transformation and are essential for predicting the environmental fate of associated trace elements.

^a Key Laboratory of Arable Land Conservation (Middle and Lower Reaches of Yangtze River), Ministry of Agriculture and Rural Affairs, College of Resources and Environment, Huazhong Agricultural University, Wuhan 430070, China.
E-mail: wangxm338@mail.hzau.edu.cn; Fax: +86 27 87288618;
Tel: +86 27 87280271

^b Department of Ecosystem Science and Management, University of Wyoming, Laramie, WY, 82071, USA

^c Univ. Grenoble Alpes, Univ. Savoie-Mont Blanc, CNRS, IRD, IFSTTAR, ISTERre, F-38000 Grenoble, France

† Electronic supplementary information (ESI) available: (1) Specific experimental conditions of the formation and transformation of schwertmannite; (2) FTIR spectra of schwertmannite obtained from the Fe^{3+} hydrolysis–dialysis pathway and of the aging products of schwertmannite formed through Fe^{3+} hydrolysis by adding NaOH; (3) XRD patterns of mineral phases obtained from Fe^{3+} hydrolysis by adding NaOH under various geochemical conditions and of the products aged for 96 h in the presence of NH_4^+ ; (4) the schwertmannite transformation rate indicated by Fe_o/Fe_t obtained from acidic dissolution experiments. See DOI: 10.1039/d0en00252f

1. Introduction

Acid mine drainage (AMD, pH < 5) is mainly generated from mining of coal and metal sulfide minerals and subsequent waste oxidative weathering, threatening the surrounding environmental quality and ecosystem equilibrium due to its low pH conditions and high concentrations of various metallic contaminants.^{1–3} AMD is usually rich in ferrous (Fe²⁺) and ferric (Fe³⁺) ions, sulfate (SO₄²⁻), and many other cations and anions, resulting in the formation of secondary iron (Fe) minerals with various ions adsorbed on their surface and/or incorporated in their structure.^{4–8} Schwertmannite is one of the most common Fe minerals in AMD, with an optimal formation pH of 2.8–4.5 and a variable chemical composition described as Fe₈O₈(OH)_{8–2x}(SO₄)_x·nH₂O (1 ≤ x ≤ 1.75).^{3,9–12} Due to its high specific surface area and tunnel structure, schwertmannite is considered as an important sink for trace elements such as As, Se, and Cr, and its formation and transformation thus affect and control the speciation, migration, and environmental fate of these trace elements in AMD environments.^{13–19}

Schwertmannite formation commonly occurs through two pathways depending on the iron sources, *i.e.*, biotic and abiotic oxidation of Fe²⁺ and direct Fe³⁺ hydrolysis.^{11,15,20–22} In AMD, it was reported that schwertmannite is mainly formed from biotic oxidation of Fe²⁺,^{7,9,23,24} hence schwertmannite formation is primarily studied in the laboratory through Fe²⁺ oxidation mediated by microbes or strong chemical oxidants, and subsequent Fe³⁺ hydrolysis–precipitation.^{3,21,23,25,26} However, in AMD-affected areas, whether schwertmannite forms through Fe²⁺ oxidation or direct Fe³⁺ hydrolysis depends on the specific solution pH and redox potential of the systems.^{27,28} Additionally, AMD often contains a mixture of Fe²⁺ and Fe³⁺,²⁹ and the regeneration of Fe³⁺ is a key process to promote the oxidation of sulfide minerals and the formation of secondary iron oxides.^{29,30} Therefore, direct Fe³⁺ hydrolysis can be an important schwertmannite formation pathway, especially when AMD solution comes into contact with surface water or infiltrates soils. However, the formation of schwertmannite through direct Fe³⁺ hydrolysis under various geochemical conditions has not been systematically investigated.

There are two pathways to synthesize schwertmannite using direct Fe³⁺ hydrolysis, including heat-enforced Fe³⁺ hydrolysis and subsequent dialysis (hereafter referred to as Fe³⁺ hydrolysis–dialysis), and Fe³⁺ hydrolysis by adding OH[−]. Fe³⁺ hydrolysis–dialysis is a common pathway for synthesis of schwertmannite, which enforces Fe³⁺ hydrolysis at 60 °C followed by dialysis of the suspension for 30 d.^{3,6,17} However, the influence of Fe³⁺ hydrolysis temperature, dialysis time, and coexistence of ions on the formation of schwertmannite is still unclear for the hydrolysis–dialysis pathway. In addition, Fe³⁺ hydrolysis by adding OH[−] has also been applied for schwertmannite synthesis. Loan *et al.*³¹ examined the formation of schwertmannite by directly mixing acidified Fe₂(SO₄)₃ solutions with NaOH at 85 °C, indicating that the

low degree of Fe³⁺ supersaturation results in the formation of schwertmannite that possibly nucleates on two-line ferrihydrite aggregates. Studies also show that schwertmannite formation from Fe³⁺ hydrolysis by adding OH[−] can occur at room temperature (RT),^{32–34} with ferrihydrite-like molecular clusters as the intermediate product.³⁴ Overall, it remains elusive how the Fe³⁺ hydrolysis rate, sulfate concentration, pH, and types of coexisting ions affect schwertmannite formation *via* Fe³⁺ hydrolysis by adding OH[−].

Schwertmannite can transform into various Fe-bearing minerals in response to changes in solution conditions. The transformation of schwertmannite is affected by various factors, such as temperature, pH, and types and concentrations of coexisting ions, as well as the formation conditions of pre-formed schwertmannite.^{35–42} Under AMD conditions, schwertmannite gradually transforms into jarosite and goethite through a dissolution–recrystallization process.^{35,36,41} Schwertmannite can also transform into mackinawite or siderite under reducing conditions^{43,44} and into a mixture of lepidocrocite and goethite in the presence of Fe²⁺ at pH 6 and under anoxic conditions.²² The schwertmannite used to study its transformation is mostly synthesized through Fe²⁺ oxidation–hydrolysis. However, the physicochemical properties of schwertmannite formed *via* Fe²⁺ oxidation–hydrolysis and direct Fe³⁺ hydrolysis exhibit significant differences, such as crystal-growth time, morphologies, electro-kinetic properties, *etc.*⁴⁵ Such differences may lead to different behaviors on the transformation of schwertmannite synthesized using these two pathways, which, however, remains unknown.

The objectives of this study are, therefore, to reveal the formation and transformation processes and properties of schwertmannite formed through direct Fe³⁺ hydrolysis (*i.e.*, Fe³⁺ hydrolysis–dialysis and Fe³⁺ hydrolysis by adding OH[−]) under various geochemical conditions. For the Fe³⁺ hydrolysis–dialysis pathway, the effects of hydrolysis temperature, dialysis time, and coexistence of K⁺ or NH₄⁺ on schwertmannite formation were examined. As to the second pathway of Fe³⁺ hydrolysis by adding OH[−], the effects of the Fe³⁺ hydrolysis rate, pH, Fe/S molar ratio, and coexistence of Cl[−], K⁺, or NH₄⁺ on schwertmannite formation were investigated. Additionally, the effects of these factors, as well as aging temperature and the presence of Fe²⁺, were determined on schwertmannite transformation. The effects of coexisting ions such as Fe²⁺, Cl[−], K⁺, and NH₄⁺ were considered because they might significantly affect the mineralogical properties of schwertmannite and they commonly occur in AMD environments.^{46–48} The concentrations of dissolved Fe³⁺ and SO₄²⁻ during schwertmannite transformation were determined, and the intermediate and final products were characterized by conventional or synchrotron-based X-ray diffraction (SXRD), Fourier transform infrared spectroscopy (FTIR), high-resolution scanning electron microscopy (SEM), and acidic dissolution experiments.

2. Materials and methods

2.1 Effects of hydrolysis temperature, dialysis time, and coexistence of K^+ or NH_4^+ on schwertmannite formation through Fe^{3+} hydrolysis–dialysis

Synthesis of schwertmannite *via* Fe^{3+} hydrolysis–dialysis was conducted at 60 °C.³ Briefly, 5.4 g $FeCl_3 \cdot 6H_2O$ and 1.5 g Na_2SO_4 were added into 1 L of deionized water preheated to 60 °C, and the obtained suspension was then stirred at 60 °C for an additional 12 min. The suspension was subsequently cooled to RT and dialyzed for 7 d with a final conductivity $<20 \mu S cm^{-1}$. Finally, the suspension was centrifuged, freeze-dried, ground, and stored at 4 °C before being characterized by XRD, SEM, and FTIR. To investigate the hydrolysis temperature effect, similar experiments were performed at 25 °C, 40 °C, 50 °C, 70 °C, and 80 °C. In addition, the influence of dialysis time (1, 3, 7, 10, and 15 d with hydrolysis temperatures of 25 °C and 60 °C) and the additional presence of K^+ or NH_4^+ (hydrolysis temperature of 60 °C and dialysis time of 7 d) on schwertmannite formation was also investigated. The initial molar ratio of Fe/S ($Fe/S = 2$) was the same in all experiments. All reaction conditions for the formation and transformation of schwertmannite are summarized in Table S1.†

The S and Fe contents in the final dried products were measured by dissolving 10 mg solids in 10 mL of 0.2 M acidic ammonium oxalate solution $[(NH_4)_2C_2O_4, pH 3]$.⁴⁹ The concentrations of Fe and SO_4^{2-} in the solution were determined using the modified 1,10-phenanthroline colorimetric method⁵⁰ and ion chromatography (Dionex ICS-1100), respectively.

2.2 Formation and transformation of schwertmannite through Fe^{3+} hydrolysis by adding NaOH in simulated AMD environments

AMD is acidic (usually pH 2–3.5) and rich in ferrous (Fe^{2+}), ferric (Fe^{3+}), and sulfate (SO_4^{2-}) ions with total Fe and SO_4^{2-} concentrations, respectively, ranging from 500–4500 $mg L^{-1}$ and 2000–6000 $mg L^{-1}$.⁷ Thus, to simulate AMD environments, the pH and dissolved Fe^{3+} and SO_4^{2-} concentrations used in this study were largely varied in these ranges.

2.2.1 Initial phase evolution during Fe^{3+} hydrolysis. To determine the initial phase evolution during Fe^{3+} hydrolysis, 2 mL of 0.8 M NaOH was rapidly mixed with an equal volume of 0.4 M $Fe_2(SO_4)_3$ in a 10 mL tube ($OH^-/Fe^{3+} = 1$, $Fe/S = 0.67$, $\sim pH 2.5$). The mixed solution was hydrolyzed at 25 °C for different durations (3.2, 8.7, 45, 50, 59, 70, and 140 min) in different tubes. The obtained suspensions were washed with deionized water, air dried, ground, stored at 4 °C, and then analyzed by SXRD and pair distribution function (PDF) at beamline 11-ID-B at Advanced Photon Source (APS).

To further clarify the effects of SO_4^{2-} distribution on the transformation of ferrihydrite to schwertmannite, the pre-formed ferrihydrite suspension was aged in the presence of SO_4^{2-} under the same solution conditions. Specifically, the SO_4^{2-} solution was added to 50 mL of freshly synthesized

ferrihydrite suspension, with pH 2.5, an Fe/S molar ratio of 0.67 and a final volume of 200 mL. After that, the ferrihydrite suspension was aged for the same durations (3.2, 8.7, 45, 50, 59, 70, and 140 min) under stirring.

2.2.2 Effects of the Fe^{3+} hydrolysis rate on the formation and long-term aging of schwertmannite. 126 mL of 0.2 M NaOH was added dropwise to a 74 mL mixed solution containing $Fe(NO_3)_3$ and Na_2SO_4 with an Fe/S molar ratio of 2 [$c(Fe^{3+}) = 48.55 mM$, $c(SO_4^{2-}) = 24.275 mM$] at addition rates of 0.5, 0.1, and 0.05 $mL min^{-1}$, respectively, corresponding Fe^{3+} hydrolysis rates of 33.33, 6.67, and 3.33 $\mu M min^{-1}$. In addition, NaOH was once directly added into the mixed solution of $Fe(NO_3)_3$ and Na_2SO_4 , labeled as “mixed directly”, to approximately represent an infinite Fe^{3+} hydrolysis rate. Then, the obtained mineral suspension from different Fe^{3+} hydrolysis rates was further stirred for ~ 30 min with pH kept at 3. In addition, to determine the effects of Fe^{2+} on schwertmannite transformation, an Fe^{2+} solution [$c(Fe^{3+})/c(Fe^{2+}) = 10$] was added to the fresh schwertmannite suspension formed from the condition of a NaOH addition rate of 0.1 $mL min^{-1}$. Subsequently, all the samples were sealed and aged at 60 °C for 96 h, during which, the solution pH was maintained at pH 3 by adding 0.1 M NaOH or HNO_3 at regular time intervals. The containers were open to air during pH adjustment and sampling, allowing entrance of atmospheric O_2 to the reaction systems. At pre-set time intervals, a 15 mL suspension was sampled and passed through a 0.22 μm membrane filter mounted on a vacuum apparatus. The dissolved SO_4^{2-} and Fe concentrations in the filtrates were measured as described above, whereas the wet solids on the membrane were rinsed with 30 mL deionized water, air dried, ground, and analyzed by XRD, FTIR, SEM, and acidic dissolution.

2.2.3 Effects of pH, Fe/S molar ratio, and temperature on the long-term aging of schwertmannite. Solutions containing $Fe(NO_3)_3$ and Na_2SO_4 with Fe/S molar ratios of 1.5, 2.0, 2.5, 5.0, 8.0 or 10.0 [$c(Fe^{3+}) = 48.55 mM$] were directly mixed with different amounts of 0.2 M NaOH solution, leading to final pH values of pH 2.0, 2.5, 3.0 and 3.5 with a total suspension volume of 200 mL. The suspensions with different pH values and an Fe/S molar ratio of 2.0 were aged at 80 °C for 96 h, while the suspensions with different Fe/S molar ratios were aged at 60 °C and pH 3 for 96 h. The pH effects were measured at 80 °C because a relatively high temperature favors the hydrolysis and precipitation of Fe^{3+} at low pH (*i.e.*, pH 2 and 2.5). Subsequent experimental details are the same as those in section 2.2.2.

2.2.4 Effects of co-existing Cl^- , K^+ , or NH_4^+ on the long-term aging of schwertmannite. 0.2 M NaOH solution was directly added into the mixed solutions containing $Fe(NO_3)_3$, Na_2SO_4 , and NaCl [$c(Fe^{3+}) = 48.55 mM$, $Fe/S = 2$, $Fe/Cl = 2$, 0.2] to obtain schwertmannite suspensions with a total volume of 200 mL. The schwertmannite suspensions were then aged at 60 °C and pH 3 for 96 h. In addition, solutions containing $Fe(NO_3)_3$, K_2SO_4 or $(NH_4)_2SO_4$ [$c(Fe^{3+}) = 48.55 mM$, $Fe/S = 2$ and 0.2, Fe/K^+ or $NH_4^+ = 1$ and 0.1] were directly

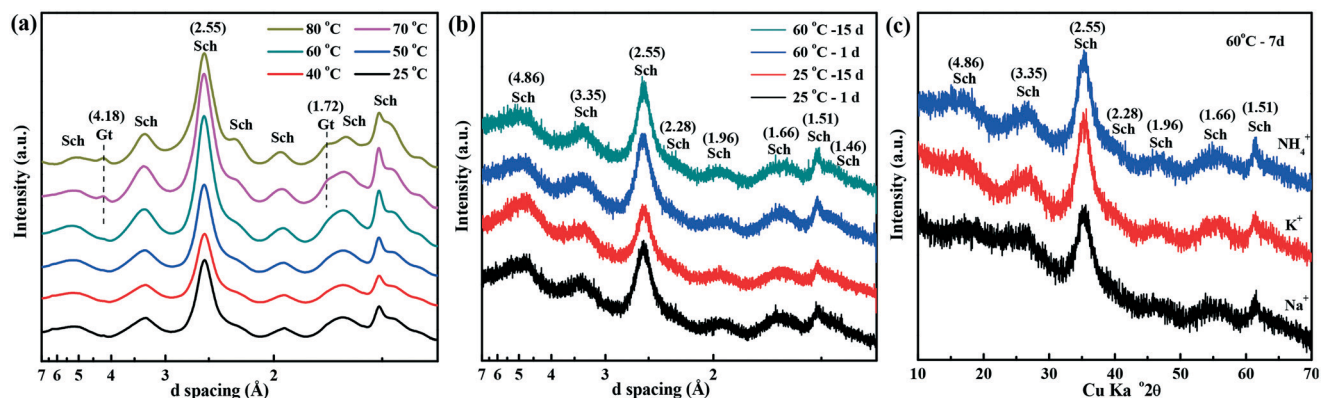


Fig. 1 XRD patterns of the products obtained from Fe^{3+} hydrolysis–dialysis at different Fe^{3+} hydrolysis temperatures followed by dialysis for 7 d (a), from Fe^{3+} hydrolysis at 25 or 60 °C followed by dialysis for 1 d or 15 d (b), and from Fe^{3+} hydrolysis at 60 °C in the presence of K^+ or NH_4^+ followed by dialysis for 7 d (c) (Gt = goethite; Sch = schwertmannite).

mixed with 0.2 M NaOH solution to obtain schwertmannite suspensions. The suspensions were subsequently aged at 80 °C and pH 2 for 96 h. Subsequent experimental details are the same as those in section 2.2.2.

2.2.5 Acidic dissolution experiments. To explore the transformation rate of schwertmannite, formed through Fe^{3+} hydrolysis by adding NaOH, under different aging conditions, 10 mg of dried intermediate sample during schwertmannite transformation was dissolved in 10 mL of 0.2 M acidic ammonium oxalate solution (pH 3, Fe_o) or 4 M HCl solution (Fe_t) at RT on a rotator for 2 h. The resulting solution was then immediately filtered through a 0.22 μm membrane. The Fe concentration in the solution was measured using a modified 1,10-phenanthroline colorimetric method.⁵⁰ The ratio of $\text{Fe}_\text{o}/\text{Fe}_\text{t}$ can reflect the transformation rate of schwertmannite, with a lower ratio indicating a faster transformation, and *vice versa*.

2.3 Solid characterization

Conventional XRD patterns for phase identification were recorded from 10 to 70° at a scan speed of 1° min^{−1} on a Bruker D8 Advance X-ray diffractometer equipped with a LynxEye detector using Ni-filtered Cu K α radiation ($\lambda = 0.15418$ nm). To identify mineral phases with poor crystallinity, synchrotron-based XRD data of some samples were collected at beamline BL14B1 ($\lambda = 0.6895$ Å, scanning from 0.5 to 30° and exposure time of 30 s) at the Shanghai Synchrotron Radiation Facility (SSRF)⁵¹ or at beamline 11-ID-B at Advanced Photon Source (APS), Argonne National Laboratory (X-ray energy of 58.86 keV, $\lambda = 0.2112$ Å).⁴⁹

The morphology and particle size of the samples were observed by SEM (SU8000) at an accelerating voltage of 10 or 20 kV. Specifically, a small amount of sample was pasted on conductive glue, and then plated using a sputtering apparatus. In addition, the FTIR spectra of the samples were recorded on a Bruker VERTEX 70 spectrophotometer. The samples were mixed gently with KBr (~1% sample weight) in an agate mortar and pelletized. 128 scans with a resolution

of 4 cm^{−1} in the range of 4000–400 cm^{−1} were collected for each sample against the air background.

3. Results and discussion

3.1 Formation of schwertmannite through Fe^{3+} hydrolysis–dialysis

The XRD patterns of the products obtained from different Fe^{3+} hydrolysis temperatures are shown in Fig. 1a. With increasing hydrolysis temperature from 25–60 °C, pure schwertmannite is obtained, and its crystallinity gradually increases, which is evidenced by the enhanced peak intensity at 2.55 Å (Fig. 1a). The chemical compositions of the products show that a higher hydrolysis temperature (25–60 °C) leads to a higher SO_4^{2-} content and a lower Fe/S ratio (Table 1), suggesting that the schwertmannite crystallinity might be related to the sulfate content,³ *i.e.*, a higher sulfate content leads to an increased crystallinity. At 25 °C, schwertmannite is flower-shaped and composed of small thin plates (Fig. 2a). With increasing hydrolysis temperature, the thin plates transform into long strips, connecting into a “sea-urchin”-like structure (Fig. 2a–d). When the hydrolysis temperature increases to 70 °C and above, minor amounts of goethite impurities form, evidenced by its characteristic peaks at 4.18 Å and 1.72 Å (Fig. 1a), while the

Table 1 The Fe and S contents in the schwertmannite samples formed at different hydrolysis temperatures, dialysis times, and in the presence of K^+ or NH_4^+

Sample	Fe	SO ₄	Molar ratio of Fe/S
	(mmol g ⁻¹)		
25 °C – 7 d	10.69	1.71	6.25
40 °C – 7 d	10.27	1.78	5.77
50 °C – 7 d	10.65	1.86	5.73
60 °C – 7 d	10.52	2.03	5.18
70 °C – 7 d	10.28	1.73	5.94
25 °C – 15 d	11.55	1.67	6.92
60 °C – 15 d	11.69	1.79	6.53
60 °C – 7 d – K ⁺	9.83	1.66	5.92
60 °C – 7d – NH ₄ ⁺	11.63	2.13	5.46

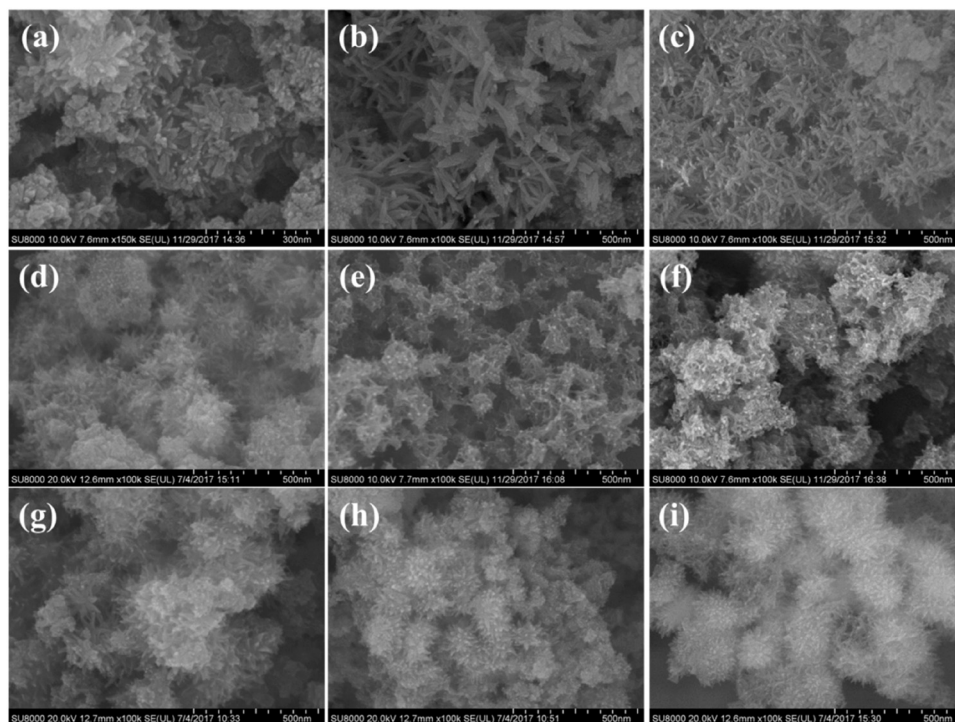


Fig. 2 SEM images of schwertmannite obtained from Fe^{3+} hydrolysis–dialysis at different hydrolysis temperatures followed by dialysis for 7 d (a–25 °C, b–40 °C, c–50 °C, d–60 °C, e–70 °C, and f–80 °C) and for different dialysis times at 25 °C (g–1 d; h–15 d) or 60 °C (i–15 d).

crystallinity of schwertmannite slightly decreases (Fig. 1a). In addition, the SO_4^{2-} content decreases and the Fe/S ratio increases (Table 1), and the long strips of schwertmannite become more clustered (Fig. 2e and f).

The FTIR spectra of these samples are similar and consistent with a typical schwertmannite IR fingerprint.^{49,52} These spectra consist of a broad triply degenerate asymmetric stretching (ν_3) band at $\sim 1125\text{ cm}^{-1}$ with two shoulder bands at ~ 1050 and $\sim 1205\text{ cm}^{-1}$, a ν_1 fundamental of the symmetric sulfate stretching at 980 cm^{-1} , a ν_4 bending band at $\sim 610\text{ cm}^{-1}$, and an Fe–O stretching band at $\sim 698\text{ cm}^{-1}$ (Fig. S1a†). Additional weak IR vibration bands at 885 cm^{-1} and 792 cm^{-1} are shown for the samples hydrolyzed at 70 °C and 80 °C, indicating the formation of minor amounts of goethite (Fig. S1a†), consistent with XRD results (Fig. 1a).

With increasing dialysis time, the diffraction peak intensities of schwertmannite slightly decrease, especially for the peak at 2.55 Å (Fig. 1b), consistent with the decrease of SO_4^{2-} content and sulfate IR band intensities (Table 1 and Fig. S1b†). In addition, schwertmannite particles aggregate more closely (Fig. 2g–i), leading to a “hedgehog” morphology.⁵³ Furthermore, compared to the Na^+ system, the presence of K^+ or NH_4^+ slightly increases the crystallinity of schwertmannite (Fig. 1c) but decreases the SO_4^{2-} content in schwertmannite (Table 1).

3.2 Mineral evolution during Fe^{3+} hydrolysis by adding NaOH

During Fe^{3+} hydrolysis in the presence of SO_4^{2-} , the XRD patterns of the intermediate products indicate that

ferrihydrate is the initial product and schwertmannite is observed later but within 45 min (Fig. 3a). Consistently, the PDF data of the initial sample (~ 3.2 min) are similar to those of the ferrihydrate reference. With increasing aging time, the intensity of the Fe–Fe peak at 5.42 Å increases, and the Fe–Fe peaks at 7.40 Å and 11.06 Å and the Fe–O peak at 6.08 Å gradually appear and increase, indicative of schwertmannite formation (Fig. 3b). In contrast, the pre-formed two-line ferrihydrate aged at the same sulfate concentration and solution pH does not transform into schwertmannite (Fig. 3c).

Sulfate-bearing ferrihydrate thus appears as an intermediate phase during the formation of schwertmannite (Fig. 3), similar to the observation of Zhu *et al.*³⁴ Transformation from ferrihydrate to schwertmannite is most likely because of the higher thermodynamic stability of schwertmannite than that of ferrihydrate.^{31,53} However, the contrast between the transformation from the intermediate ferrihydrate-like mineral (Fig. 3a) and from the pre-formed ferrihydrate (Fig. 3c) suggests that sulfate is closely associated with ferrihydrate in a way that differs from simple surface adsorption.⁵⁴ This is not unexpected because sulfate and ferrihydrate co-precipitate during Fe^{3+} hydrolysis in the presence of sulfate. The sulfate may be incorporated into the structural defects of ferrihydrate. Such a structure may have some similarity to that of schwertmannite^{3,49} and thus the formed ferrihydrate readily transforms into schwertmannite. In addition, the ferrihydrate formed in the presence of sulfate may have a smaller particle size and more structural defects

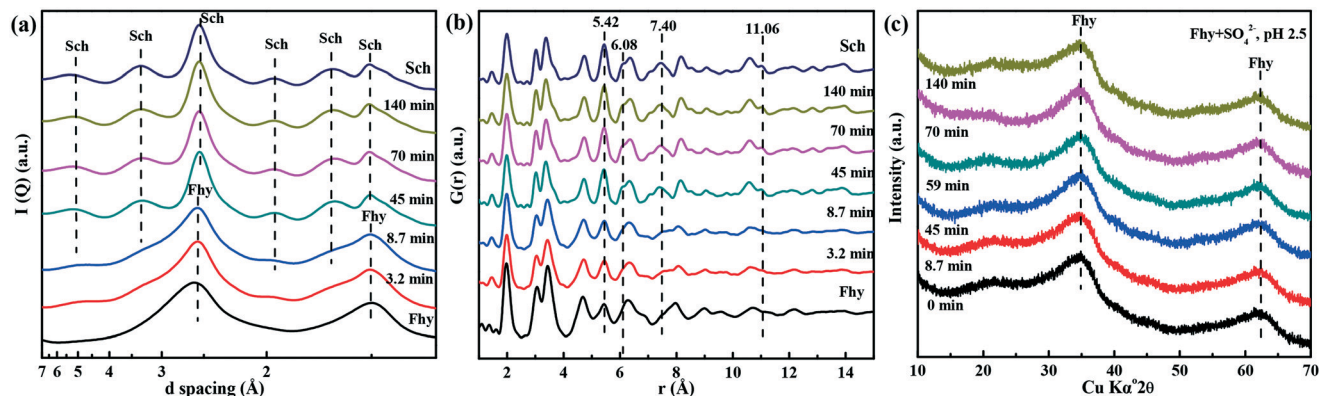
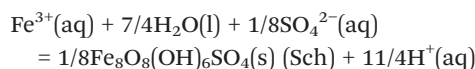


Fig. 3 Synchrotron-based XRD patterns (a) and pair distribution functions [G(r)s] (b) of the intermediate products after quickly mixing 0.8 M NaOH solution with an equal volume of 0.4 M $\text{Fe}_2(\text{SO}_4)_3$, and XRD patterns of the intermediate products for SO_4^{2-} adsorption on pre-formed ferrihydrite (c) (Sch = schwertmannite, Fhy = ferrihydrite).

than the ferrihydrite synthesized in the absence of sulfate, which further enhances its transformation to schwertmannite.⁵⁵

Schwertmannite can be formed at 25 °C through both Fe^{3+} hydrolysis–dialysis (Fig. 1) and Fe^{3+} hydrolysis by adding NaOH (Fig. 3, 4a, S2 and S3†). However, a theoretical calculation indicates that schwertmannite formation through direct Fe^{3+} hydrolysis is not thermodynamically spontaneous under ambient conditions (~ 25 °C), due to the reaction free energy ΔG_{298}° of 6.275 kJ mol^{−1} as shown in the following equation.⁷



This apparent discrepancy could be explained by the migration of protons (H^+) through the dialysis membrane into distilled water during the dialysis process. As a result, the solution pH in the dialysis bag, initially very low and

unfavorable to Fe^{3+} hydrolysis, gradually increases and then induces schwertmannite formation. On the other hand, schwertmannite readily forms from Fe^{3+} hydrolysis in the presence of sulfate by adding NaOH at 25 °C (Fig. 3 and 4), consistent with previous reports.^{32–34} Consequently, direct Fe^{3+} hydrolysis should be considered as an important pathway of schwertmannite formation in watersheds or soils surrounded by AMD with a relatively high pH.

3.3 Effects of geochemical conditions on schwertmannite formation through Fe^{3+} hydrolysis by adding NaOH

3.3.1 Effect of the Fe^{3+} hydrolysis rate. The XRD patterns indicate that pure schwertmannite forms at different Fe^{3+} hydrolysis rates, with a lower hydrolysis rate leading to an improved crystallinity (Fig. 4a). When the Fe^{3+} hydrolysis rate increases to approximate infinity (*i.e.*, “mixed directly”), the crystallinity of the product becomes very poor, but the mineral phase is indeed schwertmannite rather than

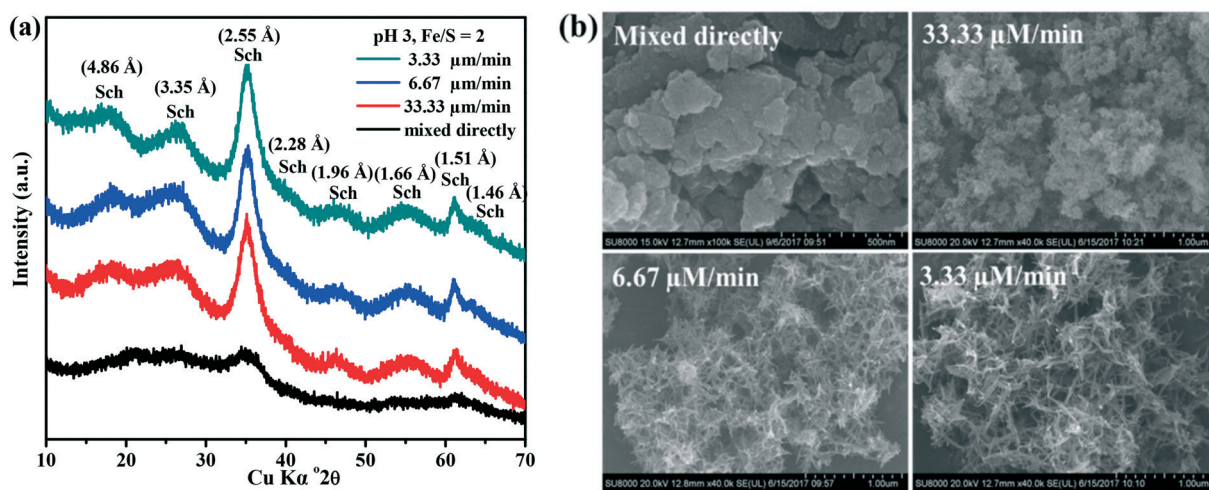


Fig. 4 XRD patterns (a) and SEM images (b) of the initial products obtained from different Fe^{3+} hydrolysis rates (mixed directly, 33.33, 6.67, and 3.33 $\mu\text{m min}^{-1}$) and pH 3. The XRD pattern of the product of “mixed directly” was enlarged and compared with that of ferrihydrite in Fig. S2.†

ferrihydrite (Fig. S2†). In addition, schwertmannite morphology varies substantially with the Fe^{3+} hydrolysis rate, exhibiting longer strips and resulting in larger and looser aggregates at a lower Fe^{3+} hydrolysis rate, similar to the sea urchin-like aggregates that form from Fe^{2+} oxidation.⁴⁵ However, the morphology obtained from the mixed directly system is a block agglomerate (Fig. 4b). These schwertmannite samples, obtained from different Fe^{3+} hydrolysis rates, should have distinct surface reactivity and geochemical behaviors, which need to be further studied.

3.3.2 Effects of pH, Fe/S molar ratio and co-existing ions. Schwertmannite can be formed through Fe^{3+} hydrolysis over a pH range of 2.0–3.5 (Fig. 4a and S3†) that is slightly wider than that of Fe^{2+} oxidation (*i.e.*, pH 2.4–3.2⁴⁵). In addition, schwertmannite can be obtained only at low initial Fe/S molar ratios ($\text{Fe/S} \leq 5$) (Fig. 3 and S3a†), *i.e.*, high sulfate concentration, while ferrihydrite forms when the Fe/S molar ratio exceeds 8, suggesting that sulfate must be present in excess, relative to the ideal mineral composition, to induce schwertmannite formation.

The XRD patterns indicate that the presence of Cl^- does not affect schwertmannite formation (Fig. S3b†), suggesting that although Cl^- can promote akaganéite ($\text{FeO}(\text{OH})_{1-x}\text{Cl}_x$) formation under acidic conditions,³⁴ the presence of abundant sulfate probably inhibits the formation of akaganéite.^{47,56} Pure schwertmannite could thus be synthesized through FeCl_3 hydrolysis–dialysis if sufficient sulfate is present.³ Additionally, the presence of K^+ or NH_4^+ slightly increases schwertmannite crystallinity (Fig. S3c†), similar to the results of the Fe^{3+} hydrolysis–dialysis pathway (Fig. 1c), probably because K^+ or NH_4^+ ions can enter the schwertmannite tunnel structure during Fe^{3+} hydrolysis, thus enhancing schwertmannite crystal growth.

3.4 Effects of geochemical conditions on the transformation of schwertmannite formed through Fe^{3+} hydrolysis by adding NaOH

3.4.1 Effect of the Fe^{3+} hydrolysis rate. During the transformation of schwertmannite formed at different Fe^{3+}

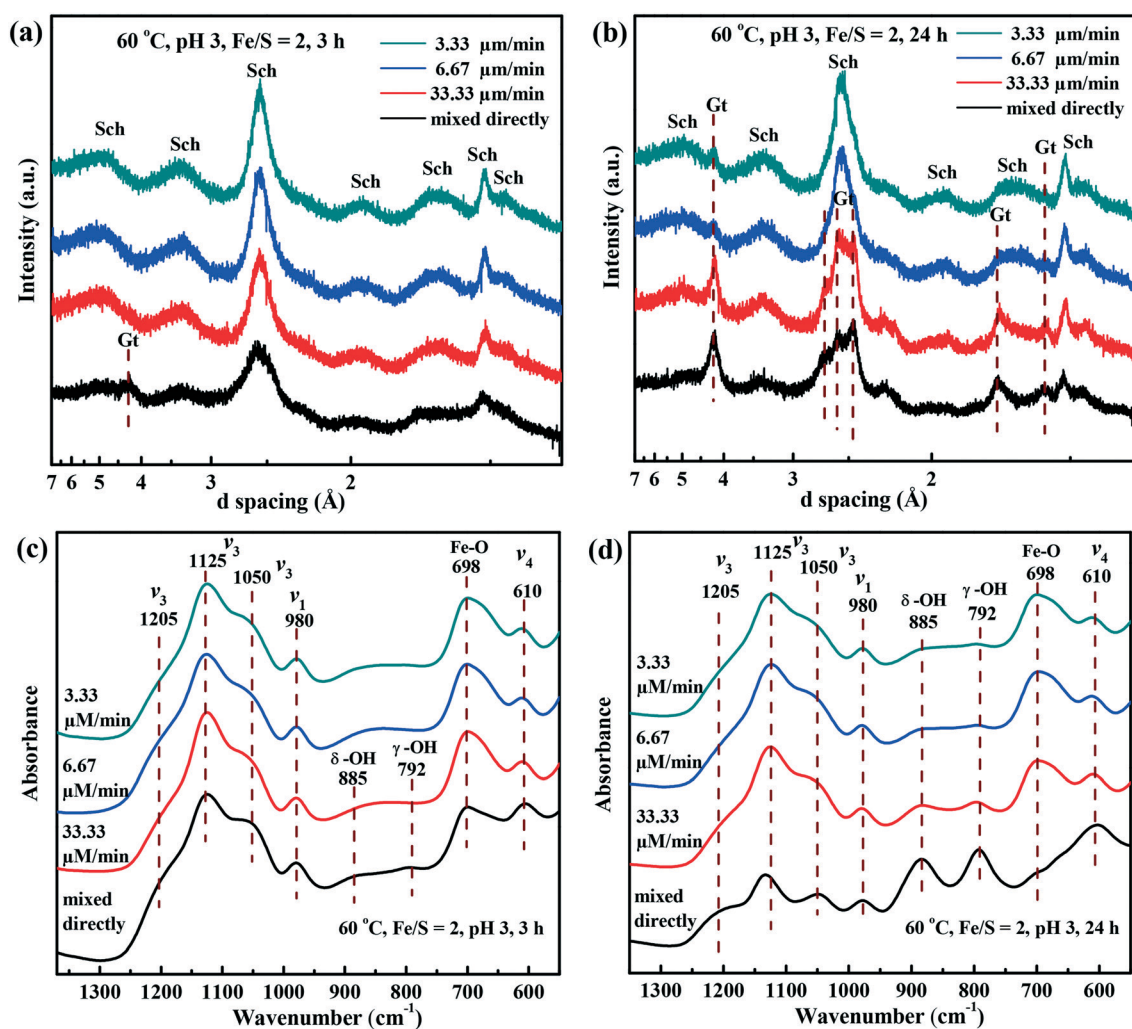


Fig. 5 Synchrotron-based XRD patterns and FTIR spectra of the products obtained from different Fe^{3+} hydrolysis rates after aging for 3 h (a and c) and 24 h (b and d) at 60 °C and pH 3 (Gt = goethite; Sch = schwertmannite).

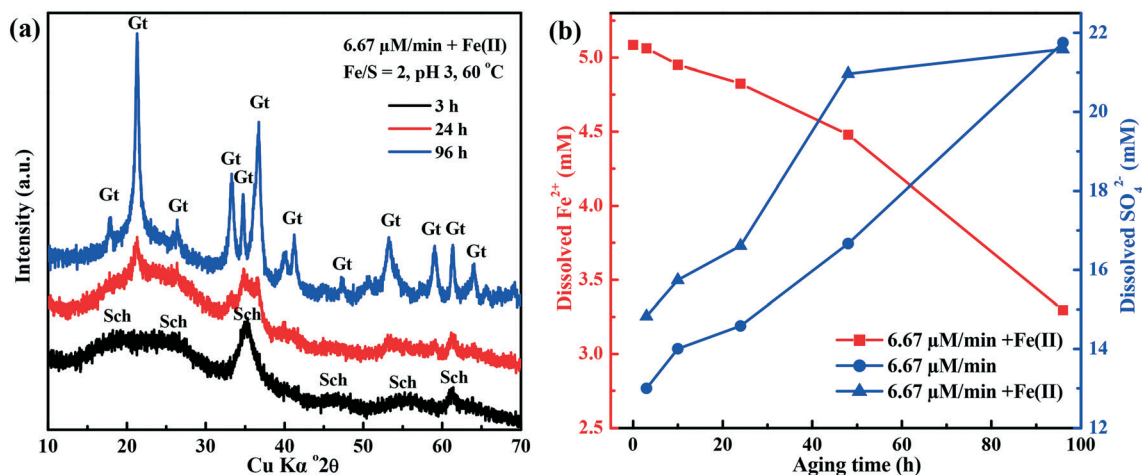


Fig. 6 XRD patterns of the aging products of schwertmannite, obtained from the Fe^{3+} hydrolysis rate of $6.67 \mu\text{M min}^{-1}$, in the presence of Fe^{2+} at pH 3 and 60 $^{\circ}\text{C}$ (a) and the concentrations of dissolved Fe^{2+} and SO_4^{2-} (mM) during the transformation (b) ($\text{Fe}^{3+}/\text{Fe}^{2+} = 10$; Gt = goethite; Sch = schwertmannite).

hydrolysis rates, minor amounts of goethite form only in the mixed directly sample after aging for 3 h (Fig. 5a). With

increasing aging time to 24 h, goethite is present in all the samples, with more goethite occurring at a higher Fe^{3+}

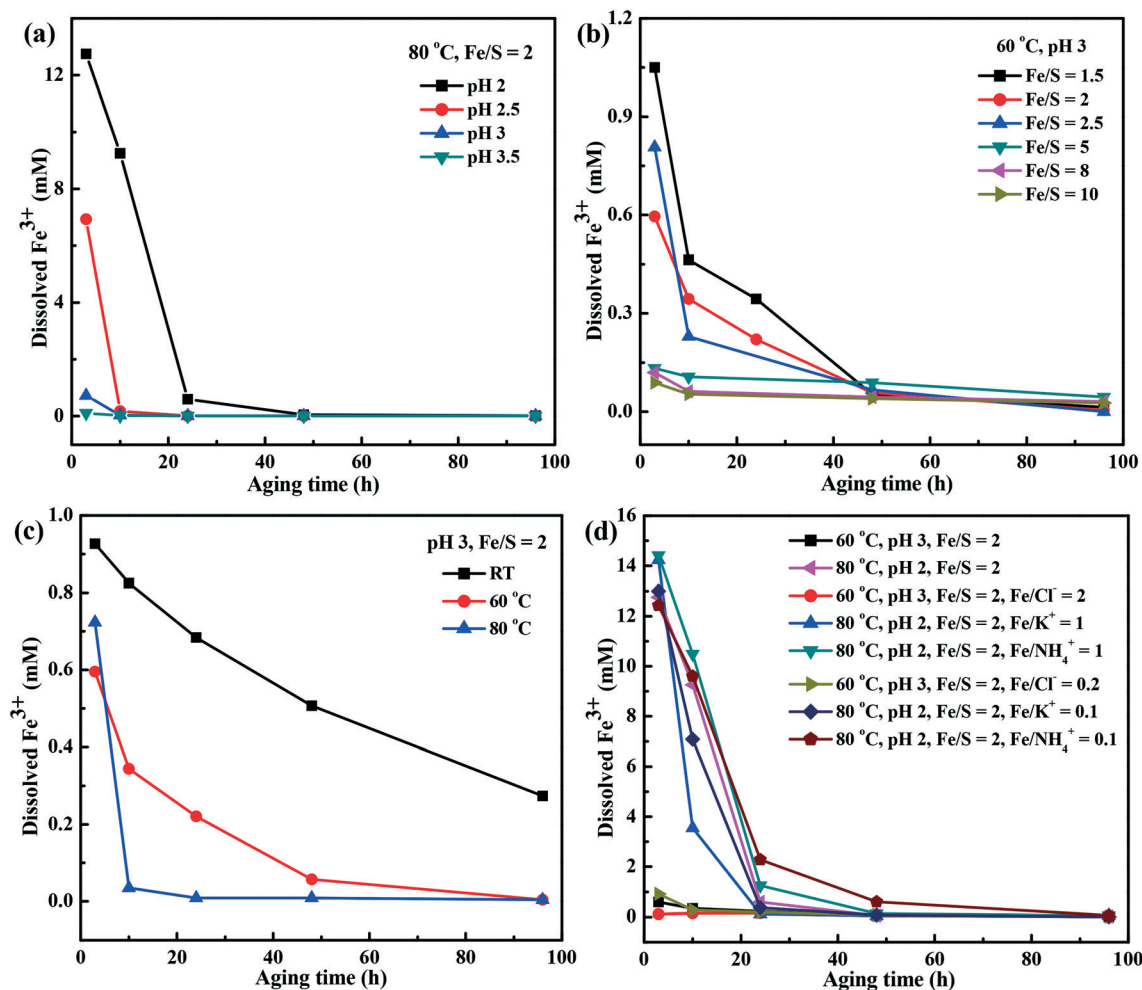


Fig. 7 Concentration of dissolved Fe^{3+} (mM) during the transformation of schwertmannite, obtained from Fe^{3+} hydrolysis by adding OH^- , over a pH range of 2.0–3.5 (a), Fe/S molar ratios of 1.5–10 (b), a temperature range of 25–80 $^{\circ}\text{C}$ (c) and in the presence of Cl^- , K^+ or NH_4^+ (d).

hydrolysis rate (Fig. 5b), suggesting that the schwertmannite obtained at a higher Fe^{3+} hydrolysis rate is less stable, possibly due to its lower crystallinity. The FTIR spectra of the samples aged for 3 h (Fig. 5c) and 24 h (Fig. 5d) show that the characteristic Fe–O stretching band of schwertmannite at $\sim 698\text{ cm}^{-1}$ decreases with aging time, whereas the characteristic OH bending vibration bands of goethite at 885 cm^{-1} and 792 cm^{-1} increase with increasing Fe^{3+} hydrolysis rate and aging time, confirming the XRD results (Fig. 5a and b). Thus, a lower Fe^{3+} hydrolysis rate leads to a larger crystallite size and a higher structural stability of schwertmannite, thereby disfavoring its transformation to other phases, such as goethite. This observation is consistent with the transformation of schwertmannite formed from Fe^{2+} oxidation.^{15,20,57}

3.4.2 Effect of the presence of Fe^{2+} . After the schwertmannite suspension was aged for 24 h, the XRD patterns indicate that goethite diffraction peaks are stronger in the presence of Fe^{2+} (Fig. 6a), compared to the Fe^{2+} -free system (Fig. 5b), suggesting that Fe^{2+} significantly accelerates schwertmannite transformation to goethite. In addition, the

concentration of dissolved SO_4^{2-} is higher in the presence of Fe^{2+} than that in the Fe^{2+} -free system (Fig. 6b), indicating that Fe^{2+} promotes the dissolution of schwertmannite and the release of sulfate. With increasing aging time, the concentration of dissolved Fe^{2+} decreases, while that of dissolved SO_4^{2-} increases (Fig. 6b), suggesting that schwertmannite transforms into goethite through a dissolution–recrystallization mechanism by consuming Fe^{2+} and releasing SO_4^{2-} . The enhancement of schwertmannite transformation in the presence of Fe^{2+} can be explained by two possible reasons. On the one hand, aqueous $\text{Fe}(\text{II})$ species can exchange structural $\text{Fe}(\text{III})$, thus enhancing the mineral phase reorganization, as evidenced by stable Fe isotope tracers.^{58–60} On the other hand, electron transfer between adsorbed $\text{Fe}(\text{II})$ and structural $\text{Fe}(\text{III})$ promotes the reductive dissolution of schwertmannite and its subsequent recrystallization.^{59,61,62}

3.4.3 Effects of pH, temperature, and Fe/S molar ratio. At $80\text{ }^\circ\text{C}$ and $\text{Fe}/\text{S} = 2$, the concentration of dissolved Fe^{3+} decreases with increasing pH from 2.0 to 3.5 (Fig. 7a), while that of dissolved SO_4^{2-} increases (Fig. 8a), indicating that a higher

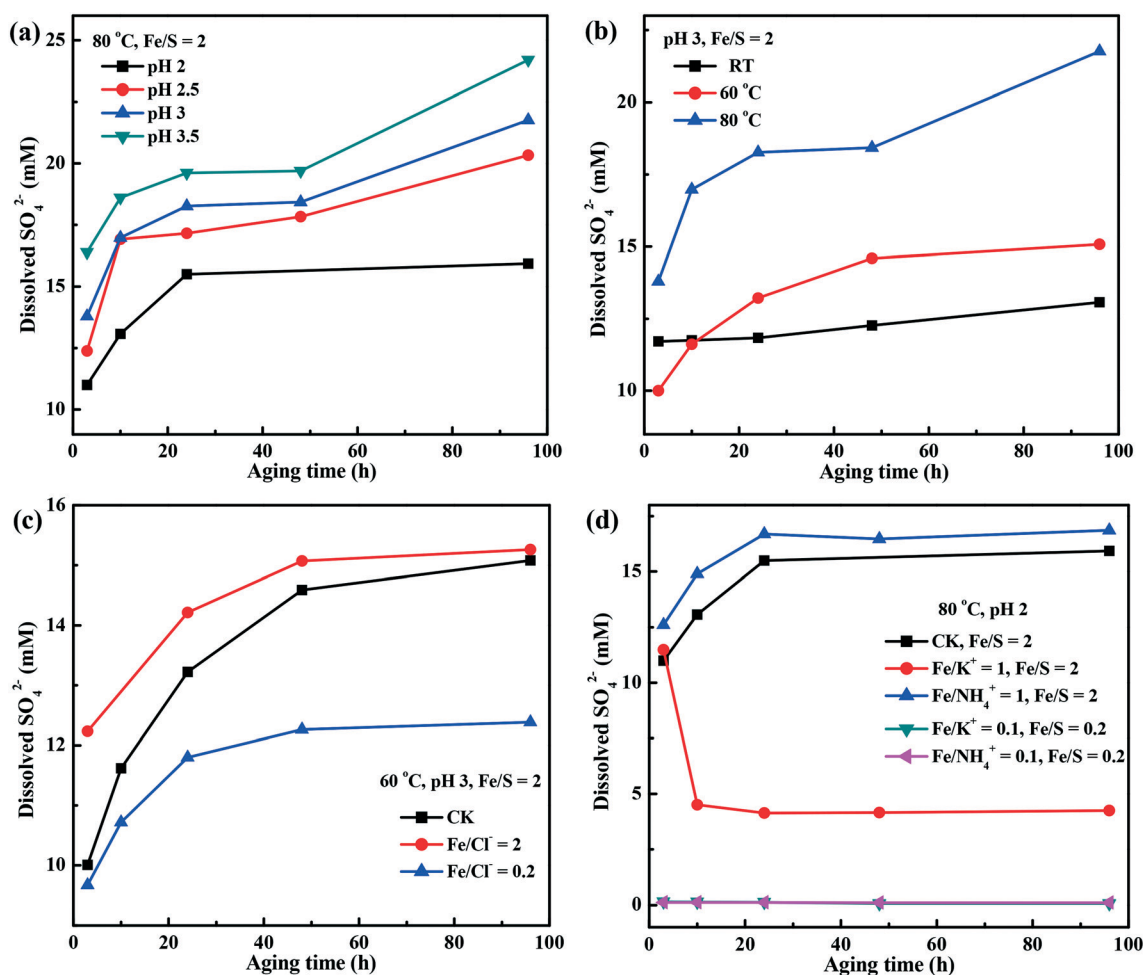


Fig. 8 Concentration of dissolved SO_4^{2-} (mM) during the transformation of schwertmannite, obtained from Fe^{3+} hydrolysis by adding OH^- , at different pH values (a), different aging temperatures (b), and in the presence of Cl^- (c) and K^+ or NH_4^+ (d).

pH enhances SO_4^{2-} release and thus the transformation of schwertmannite to goethite. This transformation is supported by XRD patterns (Fig. 9a) and the lower ratio of $\text{Fe}_\text{o}/\text{Fe}_\text{t}$ at a higher pH (Fig. S5b†). Additionally, the FTIR spectra indicate that the characteristic Fe–O stretching band of schwertmannite at $\sim 701\text{ cm}^{-1}$ gradually decreases, whereas the OH bending vibration bands of goethite at 885 cm^{-1} and 792 cm^{-1} increase with increasing pH (Fig. S4a†), further confirming the above analysis. The faster transformation rate of schwertmannite to goethite can be partially ascribed to the easier sulfate release at a higher pH.³⁵

For a given pH and Fe/S molar ratio, the concentration of dissolved Fe^{3+} substantially decreases with increasing aging temperature from 25 to 80°C and aging time (Fig. 7c). As to dissolved SO_4^{2-} , it increases slightly at 25°C and more significantly at high temperatures with increasing aging time (Fig. 8b), suggesting that SO_4^{2-} release is enhanced at a higher temperature during schwertmannite transformation. Additionally, the XRD patterns (Fig. 9c), FTIR spectra (Fig.

S4c†), and acidic dissolution results (Fig. S5a†) all indicate that goethite formation is favored at higher aging temperatures and longer aging times, consistent with lower concentration of dissolved Fe^{3+} (Fig. 7c) and higher concentration of dissolved SO_4^{2-} (Fig. 8b). Moreover, the mineral phases formed at different Fe/S molar ratios exhibit different stabilities at 60°C and pH 3 (Fig. 9b and S4b†), with a lower Fe/S molar ratio resulting in a higher concentration of dissolved Fe^{3+} (Fig. 7b). As a consequence, the schwertmannite obtained from a lower Fe/S molar ratio (Fe/S ≤ 5) transforms more readily into goethite than the ferrihydrite formed at higher Fe/S ratios (Fe/S > 5) (Fig. 9b and S4b†).

3.4.4 Effects of co-existing Cl^- , K^+ , or NH_4^+ . Compared to the system without Cl^- , the presence of Cl^- (Fe/ Cl^- = 2) accelerates the release of SO_4^{2-} (Fig. 8c), possibly because Cl^- promotes SO_4^{2-} release by ligand exchange, enhancing goethite formation (Fig. 9d). In contrast, a high concentration of Cl^- (Fe/ Cl^- = 0.2) inhibits SO_4^{2-} release and schwertmannite

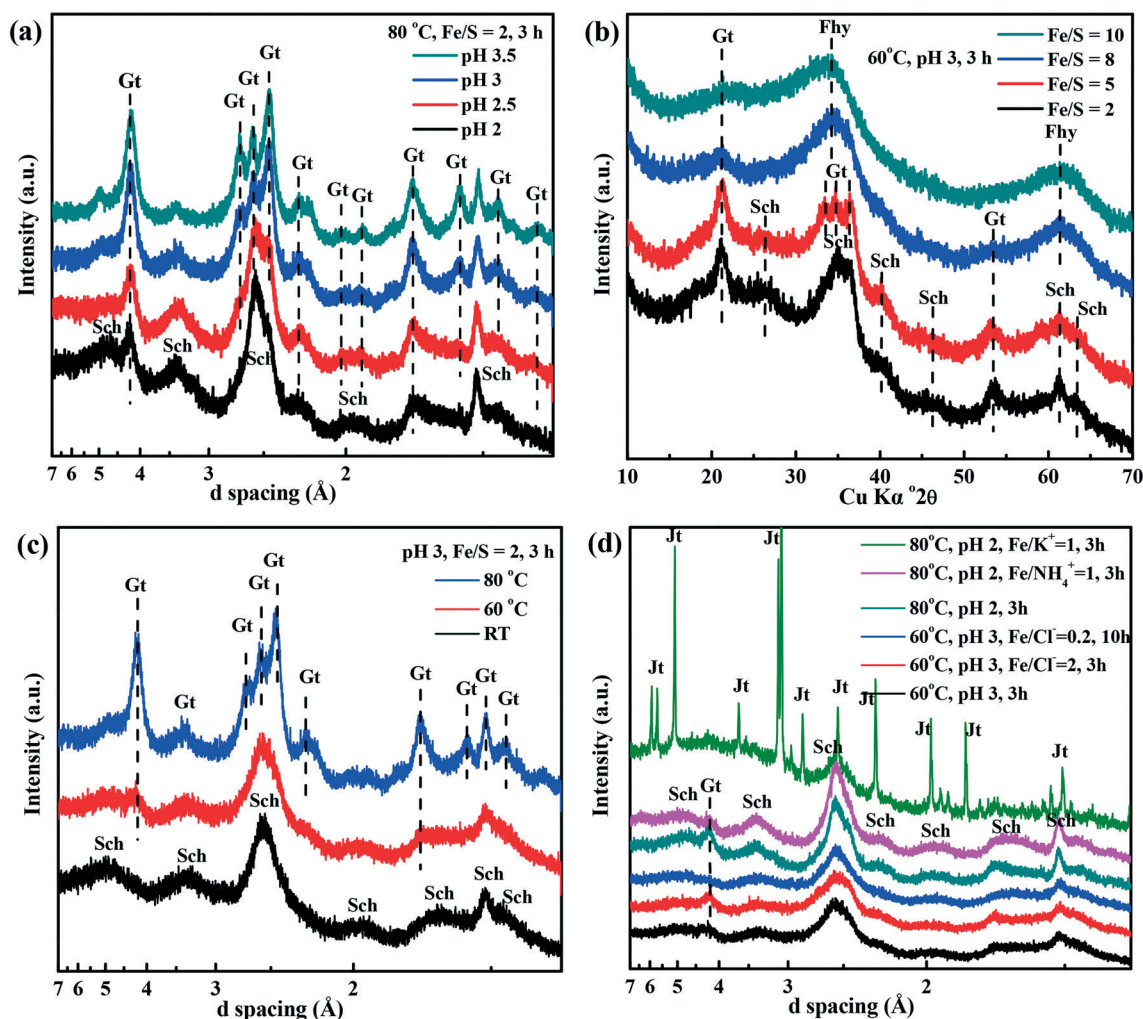


Fig. 9 XRD patterns of the schwertmannite suspension, obtained from Fe^{3+} hydrolysis by adding OH^- , aged for 3 h at different pH values (a), different Fe/S molar ratios (b), different aging temperatures (c) and in the presence of Cl^- , K^+ , or NH_4^+ (d) (Gt = goethite; Sch = schwertmannite; Fhy = ferrihydrite; Jt = jarosite).

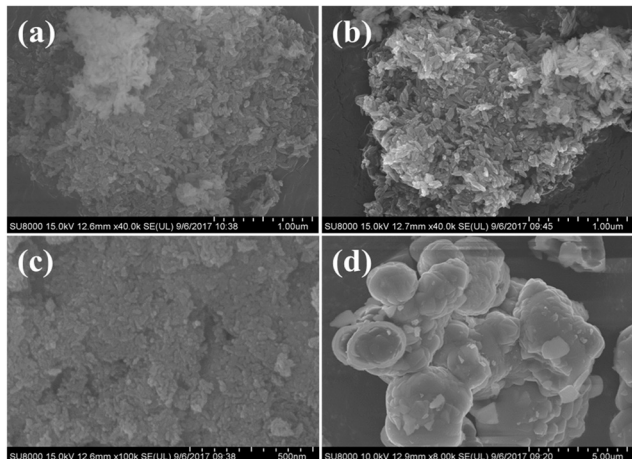


Fig. 10 SEM images of the schwertmannite suspension, obtained from Fe^{3+} hydrolysis by adding OH^- , aged for 96 h in the presence of Cl^- at 60°C or in the presence of K^+ or NH_4^+ at 80°C (a: $\text{Fe}/\text{NH}_4^+ = 1$; b: $\text{Fe}/\text{NH}_4^+ = 0.1$; c: $\text{Fe}/\text{Cl}^- = 0.2$; d: $\text{Fe}/\text{K}^+ = 0.1$).

transformation to goethite (Fig. 8c, 9d and S5c†), possibly because massive Cl^- adsorption on the schwertmannite surface impedes structural SO_4^{2-} release and thus the dissolution–recrystallization process. As reported previously, adsorption of ions on the schwertmannite surface could stabilize its structure.^{39,63}

The presence of K^+ promotes hydrolysis and precipitation of dissolved Fe^{3+} (Fig. 7d) and inhibits SO_4^{2-} release (Fig. 8d), thus facilitating the formation of K^+ -bearing jarosite with a aggregated spherical morphology (Fig. 9d and 10d). K^+ -bearing jarosite formation is also confirmed by the FTIR spectrum with characteristic bands at around $1080\text{--}1200\text{ cm}^{-1}$, 1008 cm^{-1} , and 628 cm^{-1} (Fig. S4d†), respectively, assigned to the vibrational modes of $\nu_3(\text{SO}_4^{2-})$, $\nu_1(\text{SO}_4^{2-})$, and $\nu_4(\text{SO}_4^{2-})$.⁶⁴ Similarly, a high NH_4^+ concentration ($\text{Fe}/\text{NH}_4^+ = 0.1$) also favors jarosite formation with a very low concentration of dissolved SO_4^{2-} (Fig. 8d), leading to the coexistence of goethite and NH_4^+ -bearing jarosite in the final aging products (Fig. S6†), similar to the results observed in the Fe^{2+} bio-oxidation system.^{65,66} More lath-like particles and looser aggregates are observed at a higher concentration of NH_4^+ (Fig. 10b). However, the presence of low NH_4^+ concentration ($\text{Fe}/\text{NH}_4^+ = 1$) increases the release of SO_4^{2-} (Fig. 8d), thus inducing the transformation of schwertmannite to goethite (Fig. S5c and S6†). Compared to NH_4^+ , the presence of K^+ is more easily to induce jarosite formation, consistent with a previous study indicating that the ability of K^+ to promote jarosite formation is $\sim 75\times$ greater than that of NH_4^+ ,⁶⁷ probably because the ionic radius of hydrated K^+ (1.32 \AA) fits better in the jarosite structure than that of NH_4^+ (1.44 \AA).

4. Conclusion and implications

In the present study, schwertmannite formation through direct Fe^{3+} hydrolysis and its subsequent transformation have

been systematically investigated under various geochemical conditions. Schwertmannite can be formed through Fe^{3+} hydrolysis over a temperature range of $25\text{--}60^\circ\text{C}$, a pH range of $2.0\text{--}3.5$, molar ratios of Fe/S lower than 5, Fe^{3+} hydrolysis rates higher than $3.33\text{ }\mu\text{M min}^{-1}$, and in the presence of Cl^- , K^+ or NH_4^+ (Fig. 11). Such an extended range of conditions suggests that direct Fe^{3+} hydrolysis is an important pathway for schwertmannite formation in natural AMD-affected environments, and that the chemical composition, micro-structure, and reactivity of schwertmannite vary with these geochemical conditions. In fact, schwertmannite formed through Fe^{2+} oxidation–hydrolysis also includes a process of Fe^{3+} hydrolysis–precipitation, so these new insights into schwertmannite formation through direct Fe^{3+} hydrolysis are also essential to understand the mineralization process during Fe^{2+} oxidation in AMD environments.

During schwertmannite formation through direct Fe^{3+} hydrolysis, sulfate-bearing ferrihydrite is an intermediate product and sulfate is likely incorporated into the structural defects of ferrihydrite particles, rather than being simply adsorbed on their surfaces, to induce schwertmannite formation. Due to the abundance of sulfate in AMD environments, these anions readily co-precipitate with ferrihydrite through Fe^{3+} hydrolysis, allowing for the subsequent transformation to schwertmannite and accounting for the greater occurrence of schwertmannite than ferrihydrite in AMD-affected areas.

Schwertmannite readily transforms into more stable goethite and jarosite. High temperature, high pH, and the presence of Fe^{2+} all enhance the transformation to goethite by promoting the release of structural sulfate, whereas a low Fe^{3+} hydrolysis rate and a high Cl^- concentration hinder this transformation. Moreover, the presence of K^+ or a high NH_4^+ concentration favors schwertmannite transformation to K^+ - or NH_4^+ -bearing jarosite (Fig. 11). These new insights into schwertmannite formation and transformation under various geochemical conditions are vital to understand the

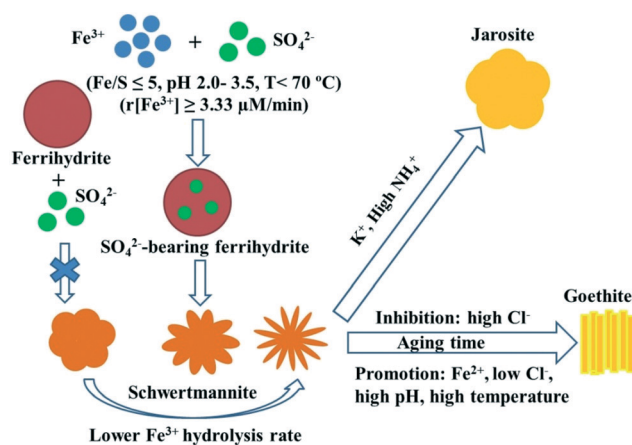


Fig. 11 Schematic diagram of schwertmannite formation and transformation through direct Fe^{3+} hydrolysis under various geochemical conditions.

mineralogical properties of schwertmannite and predict the environmental behavior and fate of trace elements associated with schwertmannite in AMD-affected environments.

Conflicts of interest

There are no conflicts to declare.

Acknowledgements

This study was supported by the National Natural Science Foundation of China (No. 41601228 and 41977021) and the Fundamental Research Funds for the Central Universities (No. 2662019QD015). The authors thank the Shanghai Synchrotron Radiation Facility (SSRF) (beamline BL14B1) and Advanced Photon Source (APS) (beamline 11-ID-B), Argonne National Laboratory (ANL), for providing the beam time and assistance during data collection.

References

- 1 G. S. Simate and S. Ndlovu, Acid mine drainage: Challenges and opportunities, *J. Environ. Chem. Eng.*, 2014, **2**, 1785–1803.
- 2 K. K. Kefeni, T. A. M. Msagati and B. B. Mamba, Acid mine drainage: Prevention, treatment options, and resource recovery: A review, *J. Cleaner Prod.*, 2017, **151**, 475–493.
- 3 J. M. Bigham, U. Schwertmann, L. Carlson and E. Murad, A poorly crystallized oxyhydroxysulfate of iron formed by bacterial oxidation of Fe(II) in acid-mine waters, *Geochim. Cosmochim. Acta*, 1990, **54**, 2743–2758.
- 4 Y. Xie, G. Lu, C. Yang, L. Qu, M. Chen, C. Guo and Z. Dang, Mineralogical characteristics of sediments and heavy metal mobilization along a river watershed affected by acid mine drainage, *PLoS One*, 2018, **13**, e0190010.
- 5 S. Paikaray, J. Gottlicher and S. Peiffer, Removal of As(III) from acidic waters using schwertmannite: Surface speciation and effect of synthesis pathway, *Chem. Geol.*, 2011, **283**, 134–142.
- 6 J. Antelo, S. Fiol, D. Gondar, R. Lopez and F. Arce, Comparison of arsenate, chromate and molybdate binding on schwertmannite: Surface adsorption vs anion-exchange, *J. Colloid Interface Sci.*, 2012, **386**, 338–343.
- 7 L. Zhou, Biomineralization: a pivotal process in developing a novel passive treatment system for acid mine drainage, *Chin. J. Chem.*, 2017, **75**, 552–559 (in chinese).
- 8 M. P. Asta, J. Cama, M. Martinez and J. Gimenez, Arsenic removal by goethite and jarosite in acidic conditions and its environmental implications, *J. Hazard. Mater.*, 2009, **171**, 965–972.
- 9 J. M. Bigham, L. Carlson and E. Murad, Schwertmannite, a new iron oxyhydroxysulphate from pyhasalmi, finland, and other localities, *Mineral. Mag.*, 1994, **58**, 641–648.
- 10 U. Schwertmann, J. M. Bigham and E. Murad, The 1st occurrence of schwertmannite in a natural stream environment, *Eur. J. Mineral.*, 1995, **7**, 547–552.
- 11 S. Regenspurg, A. Brand and S. Peiffer, Formation and stability of schwertmannite in acidic mining lakes, *Geochim. Cosmochim. Acta*, 2004, **68**, 1185–1197.
- 12 A. Fernandez-Martinez, V. Timon, G. Roman-Ross, G. J. Cuello, J. E. Daniels and C. Ayora, The structure of schwertmannite, a nanocrystalline iron oxyhydroxysulfate, *Am. Mineral.*, 2010, **95**, 1312–1322.
- 13 E. D. Burton, R. T. Bush, S. G. Johnston, K. M. Watling, R. K. Hocking, L. A. Sullivan and G. K. Parker, Sorption of arsenic(V) and arsenic(III) to schwertmannite, *Environ. Sci. Technol.*, 2009, **43**, 9202–9207.
- 14 S. Carrero, A. Fernandez-Martinez, R. Perez-Lopez, A. Poulain, E. Salas-Colera and J. M. Nieto, Arsenate and selenate scavenging by basaluminite: Insights into the reactivity of aluminum phases in acid mine drainage, *Environ. Sci. Technol.*, 2017, **51**, 28–37.
- 15 Z. Zhang, G. Guo, X. Li, Q. Zhao, X. Bi, K. Wu and H. Chen, Effects of hydrogen-peroxide supply rate on schwertmannite microstructure and chromium(VI) adsorption performance, *J. Hazard. Mater.*, 2018, **367**, 520–528.
- 16 P. Acero, C. Ayora, C. Torrento and J. M. Nieto, The behavior of trace elements during schwertmannite precipitation and subsequent transformation into goethite and jarosite, *Geochim. Cosmochim. Acta*, 2006, **70**, 4130–4139.
- 17 J. Antelo, S. Fiol, D. Gondar, C. Perez, R. Lopez and F. Arce, Cu(II) incorporation to schwertmannite: Effect on stability and reactivity under AMD conditions, *Geochim. Cosmochim. Acta*, 2013, **119**, 149–163.
- 18 C. Fan, C. Guo, Y. Zeng, Z. Tu, Y. Ji, J. R. Reinfelder, M. Chen, W. Huang, G. Lu, X. Yi and Z. Dang, The behavior of chromium and arsenic associated with redox transformation of schwertmannite in AMD environment, *Chemosphere*, 2019, **222**, 945–953.
- 19 P. Cruz-Hernández, R. Pérez-López, A. Parviainen, M. B. J. Lindsay and J. M. Nieto, Trace element-mineral associations in modern and ancient iron terraces in acid drainage environments, *Catena*, 2016, **147**, 386–393.
- 20 J. Song, S. Y. Jia, H. T. Ren, S. H. Wu and X. Han, Application of a high-surface-area schwertmannite in the removal of arsenate and arsenite, *Int. J. Environ. Sci. Technol.*, 2014, **12**, 1559–1568.
- 21 Y. Liao, L. Zhou, S. Bai, J. Liang and S. Wang, Occurrence of biogenic schwertmannite in sludge bioleaching environments and its adverse effect on solubilization of sludge-borne metals, *Appl. Geochem.*, 2009, **24**, 1739–1746.
- 22 L. Liu, Z. Jia, W. Tan, S. L. Suib, L. Ge, G. Qiu and R. Hu, Abiotic photomineralization and transformation of iron oxide nanominerals in aqueous systems, *Environ. Sci.: Nano*, 2018, **5**, 1169–1178.
- 23 M. Kawano and K. Tomita, Geochemical modeling of bacterially induced mineralization of schwertmannite and jarosite in sulfuric acid spring water, *Am. Mineral.*, 2001, **86**, 1156–1165.
- 24 W. Stumm and J. J. Morgan, *Aquatic chemistry: an introduction emphasizing chemical equilibria in natural waters*, 1970.

- 25 Y. Liao, L. Zhou, J. Liang and H. Xiong, Biosynthesis of schwertmannite by *Acidithiobacillus ferrooxidans* cell suspensions under different pH condition, *Mater. Sci. Eng., C*, 2009, **29**, 211–215.
- 26 J. S. Tischler, C. Wiacek, E. Janneck and M. Schlomann, Microbial abundance in the schwertmannite formed in a mine water treatment plant, *Mine Water Environ.*, 2013, **32**, 258–265.
- 27 D. K. Nordstrom, Hydrogeochemical processes governing the origin, transport and fate of major and trace elements from mine wastes and mineralized rock to surface waters, *Appl. Geochem.*, 2011, **26**, 1777–1791.
- 28 S. Carrero, R. Pérez-López, A. Fernandez-Martinez, P. Cruz-Hernández, C. Ayora and A. Poulain, The potential role of aluminium hydroxysulphates in the removal of contaminants in acid mine drainage, *Chem. Geol.*, 2015, **417**, 414–423.
- 29 J. G. Skousen, A. Sexstone and P. F. Ziemkiewicz, in *Acid mine drainage control and treatment*, West Virginia University and the National Mine Land Reclamation Center, Morgantown, 1996, ch. 6.
- 30 D. K. Nordstrom, D. W. Blowes and C. J. Ptacek, Hydrogeochemistry and microbiology of mine drainage: An update, *Appl. Geochem.*, 2015, **57**, 3–16.
- 31 M. Loan, W. R. Richmond and G. M. Parkinson, On the crystal growth of nanoscale schwertmannite, *J. Cryst. Growth*, 2005, **275**, E1875–E1881.
- 32 W. D. Burgos, T. Borch, L. D. Troyer, F. B. Luan, L. N. Larson, J. F. Brown, J. Lambson and M. Shimizu, Schwertmannite and Fe oxides formed by biological low-pH Fe(II) oxidation versus abiotic neutralization: Impact on trace metal sequestration, *Geochim. Cosmochim. Acta*, 2012, **76**, 29–44.
- 33 L. Reichelt and M. Bertau, Transformation of nanostructured schwertmannite and 2-line-ferrihydrite into hematite, *Z. Anorg. Allg. Chem.*, 2015, **641**, 1696–1700.
- 34 M. Zhu, B. Legg, H. Zhang, B. Gilbert, Y. Ren, J. F. Banfield and G. A. Waychunas, Early stage formation of iron oxyhydroxides during neutralization of simulated acid mine drainage solutions, *Environ. Sci. Technol.*, 2012, **46**, 8140–8147.
- 35 J. Jonsson, P. Persson, S. Sjöberg and L. Lovgren, Schwertmannite precipitated from acid mine drainage: phase transformation, sulphate release and surface properties, *Appl. Geochem.*, 2005, **20**, 179–191.
- 36 U. Schwertmann and L. Carlson, The pH-dependent transformation of schwertmannite to goethite at 25 °C, *Clay Miner.*, 2005, **40**, 63–66.
- 37 K. H. Knorr and C. Blodau, Controls on schwertmannite transformation rates and products, *Appl. Geochem.*, 2007, **22**, 2006–2015.
- 38 L. E. Davidson, S. Shaw and L. G. Benning, The kinetics and mechanisms of schwertmannite transformation to goethite and hematite under alkaline conditions, *Am. Mineral.*, 2008, **93**, 1326–1337.
- 39 E. D. Burton, S. G. Johnston, K. Watling, R. T. Bush, A. F. Keene and L. A. Sullivan, Arsenic effects and behavior in association with the Fe(II)-catalyzed transformation of schwertmannite, *Environ. Sci. Technol.*, 2010, **44**, 2016–2021.
- 40 E. D. Burton and S. G. Johnston, Impact of silica on the reductive transformation of schwertmannite and the mobilization of arsenic, *Geochim. Cosmochim. Acta*, 2012, **96**, 134–153.
- 41 J. Sanchez-Espana, I. Yusta and G. A. Lopez, Schwertmannite to jarosite conversion in the water column of an acidic mine pit lake, *Mineral. Mag.*, 2012, **76**, 2659–2682.
- 42 S. Paikaray and S. Peiffer, Dissolution kinetics of sulfate from schwertmannite under variable pH conditions, *Mine Water Environ.*, 2010, **29**, 263–269.
- 43 E. D. Burton, R. T. Bush, L. A. Sullivan and D. R. G. Mitchell, Reductive transformation of iron and sulfur in schwertmannite-rich accumulations associated with acidified coastal lowlands, *Geochim. Cosmochim. Acta*, 2007, **71**, 4456–4473.
- 44 S. G. Johnston, E. D. Burton and E. M. Moon, Arsenic Mobilization Is Enhanced by Thermal Transformation of Schwertmannite, *Environ. Sci. Technol.*, 2016, **50**, 8010–8019.
- 45 Z. Zhang, X. Bi, X. Li, Q. Zhao and H. Chen, Schwertmannite: occurrence, properties, synthesis and application in environmental remediation, *RSC Adv.*, 2018, **8**, 33583–33599.
- 46 H. M. Wang, J. M. Bigham and O. H. Tuovinen, Formation of schwertmannite and its transformation to jarosite in the presence of acidophilic iron-oxidizing microorganisms, *Mater. Sci. Eng., C*, 2006, **26**, 588–592.
- 47 H. Xiong, Y. Liao and L. Zhou, Influence of chloride and sulfate on formation of akaganéite and schwertmannite through ferrous biooxidation by *acidithiobacillus ferrooxidans* cells, *Environ. Sci. Technol.*, 2008, **42**, 8681–8686.
- 48 S. Paikaray, C. Schröder and S. Peiffer, Schwertmannite stability in anoxic Fe(II)-rich aqueous solution, *Geochim. Cosmochim. Acta*, 2017, **217**, 292–305.
- 49 X. Wang, C. Gu, X. Feng and M. Zhu, Sulfate local coordination environment in schwertmannite, *Environ. Sci. Technol.*, 2015, **49**, 10440–10448.
- 50 E. D. Burton, R. T. Bush, L. A. Sullivan and D. R. G. Mitchell, Schwertmannite transformation to goethite via the Fe(II) pathway: Reaction rates and implications for iron-sulfide formation, *Geochim. Cosmochim. Acta*, 2008, **72**, 4551–4564.
- 51 T. Yang, W. Wen, G. Yin, X. Li, M. Gao, Y. Gu, L. Li, Y. Liu, H. Liu, X. Zhang, B. Zhao, T. Liu, Y. Yang, Z. Li, X. Zhou and X. Gao, Introduction of the X-ray diffraction beamline of SSRF, *Nucl. Sci. Tech.*, 2015, **26**, 020101.
- 52 J. F. Boily, P. L. Gassman, T. Peretyazhko, J. Szanyi and J. M. Zachara, FTIR spectral components of schwertmannite, *Environ. Sci. Technol.*, 2010, **44**, 1185–1190.
- 53 M. Loan, J. M. Cowley, R. Hart and G. M. Parkinson, Evidence on the structure of synthetic schwertmannite, *Am. Mineral.*, 2004, **89**, 1735–1742.
- 54 C. Gu, Z. Wang, J. D. Kubicki, X. Wang and M. Zhu, X-ray absorption spectroscopic quantification and speciation modeling of sulfate adsorption on ferrihydrite surfaces, *Environ. Sci. Technol.*, 2016, **50**, 8067–8076.

- 55 D. Zhang, S. Wang, Y. Wang, M. A. Gomez, Y. Duan and Y. Jia, The transformation of two-line ferrihydrite into crystalline products: effect of pH and media (sulfate versus nitrate), *ACS Earth Space Chem.*, 2018, **2**, 577–587.
- 56 T. Ishikawa, S. Miyamoto, K. Kandori and T. Nakayama, Influence of anions on the formation of β -FeOOH rusts, *Corros. Sci.*, 2005, **47**, 2510–2520.
- 57 F. Liu, J. Zhou, S. Zhang, L. Liu, L. Zhou and W. Fan, Schwertmannite synthesis through ferrous ion chemical oxidation under different H_2O_2 supply rates and its removal efficiency for arsenic from contaminated groundwater, *PLoS One*, 2015, **10**, e0138891.
- 58 A. J. Friedrich, M. Helgeson, C. Liu, C. Wang, K. M. Rosso and M. M. Scherer, Iron atom exchange between hematite and aqueous Fe(II), *Environ. Sci. Technol.*, 2015, **49**, 8479–8486.
- 59 C. Liu, Z. Zhu, F. Li, T. Liu, C. Liao, J. J. Lee, K. Shih, L. Tao and Y. Wu, Fe(II)-induced phase transformation of ferrihydrite: The inhibition effects and stabilization of divalent metal cations, *Chem. Geol.*, 2016, **444**, 110–119.
- 60 A. Neumann, L. Wu, W. Li, B. L. Beard, C. M. Johnson, K. M. Rosso, A. J. Friedrich and M. M. Scherer, Atom exchange between aqueous Fe(II) and structural Fe in clay minerals, *Environ. Sci. Technol.*, 2015, **49**, 2786–2795.
- 61 P. Larese-Casanova, A. Kappler and S. B. Haderlein, Heterogeneous oxidation of Fe(II) on iron oxides in aqueous systems: Identification and controls of Fe(III) product formation, *Geochim. Cosmochim. Acta*, 2012, **91**, 171–186.
- 62 A. M. Jones, R. N. Collins and T. D. Waite, Redox characterization of the Fe(II)-catalyzed transformation of ferrihydrite to goethite, *Geochim. Cosmochim. Acta*, 2017, **218**, 257–272.
- 63 V. A. Schoepfer, E. D. Burton and S. G. Johnston, Contrasting effects of phosphate on the rapid transformation of schwertmannite to Fe(III) (oxy)hydroxides at near-neutral pH, *Geoderma*, 2019, **340**, 115–123.
- 64 K. Sasaki, O. Tanaike and H. Konno, Distinction of jarosite-group compounds by raman spectroscopy, *Can. Mineral.*, 1998, **36**, 1225–1235.
- 65 F. S. Jones, J. M. Bigham, J. P. Gramp and O. H. Tuovinen, Synthesis and properties of ternary (K, NH_4 , H_3O)-jarosites precipitated from *Acidithiobacillus ferrooxidans* cultures in simulated bioleaching solutions, *Mater. Sci. Eng., C*, 2014, **44**, 391–399.
- 66 F. S. Jones, J. M. Bigham, J. P. Gramp and O. H. Tuovinen, Formation and characterization of ternary (Na, NH_4 , H_3O)-jarosites produced from *Acidithiobacillus ferrooxidans* cultures, *Appl. Geochem.*, 2018, **91**, 14–22.
- 67 S. Bai, Z. Xu, M. Wang, Y. Liao, J. Liang, C. Zheng and L. Zhou, Both initial concentrations of Fe(II) and monovalent cations jointly determine the formation of biogenic iron hydroxysulfate precipitates in acidic sulfate-rich environments, *Mater. Sci. Eng., C*, 2012, **32**, 2323–2329.

Electronic supplementary information

Formation and transformation of schwertmannite through direct Fe³⁺ hydrolysis under various geochemical conditions

Hong Ying^a, Xionghan Feng^a, Mengqiang Zhu^b, Bruno Lanson^c, Fan Liu^a, Xiaoming
Wang^{a,*}

^a Key Laboratory of Arable Land Conservation (Middle and Lower Reaches of Yangtze River), Ministry of Agriculture, College of Resources and Environment, Huazhong Agricultural University, Wuhan 430070, China

^b Department of Ecosystem Science and Management, University of Wyoming, Laramie, WY, 82071, United States of America

^c Univ. Grenoble Alpes, Univ. Savoie-Mont Blanc, CNRS, IRD, IFSTTAR, ISTERre, F-38000 Grenoble, France

Supplementary data includes 1 table and 6 figures.

*Corresponding author:

Xiaoming Wang, Tel: +86 27 87280271; Fax: +86 27 87288618; E-mail:
wangxm338@mail.hzau.edu.cn

Table S1. Experimental conditions on formation and transformation of schwertmannite through direct Fe^{3+} hydrolysis

Sample	Fe^{3+} (mM)	SO_4^{2-} (mM)	pH	Temperature	Co-existing ions (mM)	Dialysis time
(a) Schwertmannite formation through Fe^{3+} hydrolysis-dialysis pathway						
Hydrolysis temperature	19.98	10.56	-	25, 40, 50, 60, 70, 80 °C	-	7d
Dialysis time	19.98	10.56	-	25, 60 °C	-	1, 3, 7, 15 d
Coexistence of K^+ or NH_4^+	19.98	10.56	-	60 °C	K^+ , NH_4^+ (21.12 mM)	7d
(b) Mineral evolution during Fe^{3+} hydrolysis by adding NaOH						
$\text{OH}^-/\text{Fe}^{3+} = 1$	400	600	2.5	25 °C	-	-
$\text{Fhy} + \text{SO}_4^{2-}$	48.55	72.825	2.5	25 °C	-	-
(c) Fe^{3+} hydrolysis rate on the formation and long-term aging of schwertmannite						
33.33 $\mu\text{M}/\text{min}$	48.55	24.275	3.0	Formed: 25 °C Aging: 60 °C	-	-
6.67 $\mu\text{M}/\text{min}$	48.55	24.275	3.0	Formed: 25 °C Aging: 60 °C	-	-
3.33 $\mu\text{M}/\text{min}$	48.55	24.275	3.0	Formed: 25 °C Aging: 60 °C	-	-
(d) Schwertmannite transformation under various geochemical conditions						
pH effects	48.55	24.275	2.0, 2.5, 3.0, 3.5	Aging: 80 °C	-	-
Fe/S molar ratios	48.55	32.37, 24.275, 19.42, 9.71, 6.07, 4.855	3.0	Aging: 60 °C	-	-

Aging temperature	48.55	24.275	3.0	25, 60, 80 °C	-	-
Co-existing Fe^{2+}	48.55	24.275	3.0	Aging: 60 °C	Fe^{2+} (4.855 mM)	-
Co-existing Cl^-	48.55	24.274	3.0	Aging: 60 °C	Cl^- (24.275, 242.75 mM)	-
Co-existing K^+ or NH_4^+	48.55	24.275, 247.25	2.0	Aging: 80 °C	K^+ , NH_4^+ (48.55, 485.5 mM)	-

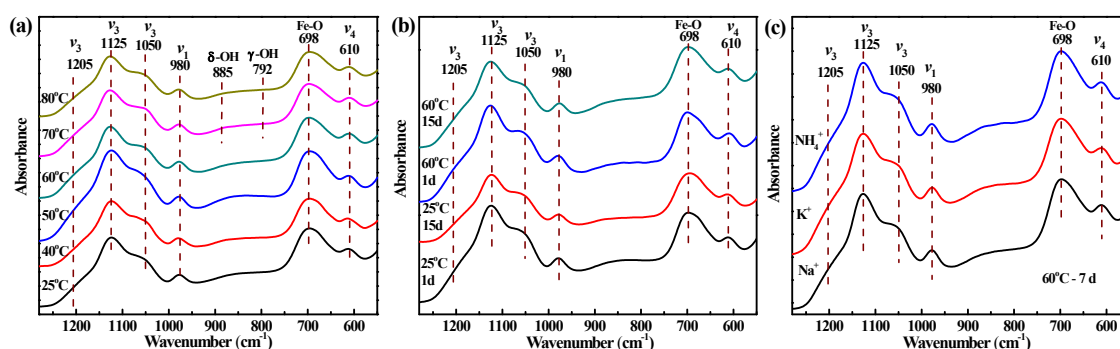


Fig. S1. FTIR spectra of the products obtained from Fe^{3+} hydrolysis-dialysis at different Fe^{3+} hydrolysis temperatures followed by dialysis for 7 d (a), from Fe^{3+} hydrolysis at 25 °C or 60 °C followed by dialysis for 1 d or 15 d (b), and from Fe^{3+} hydrolysis at 60 °C in the presence of K^+ or NH_4^+ followed by dialysis for 7 d (c).

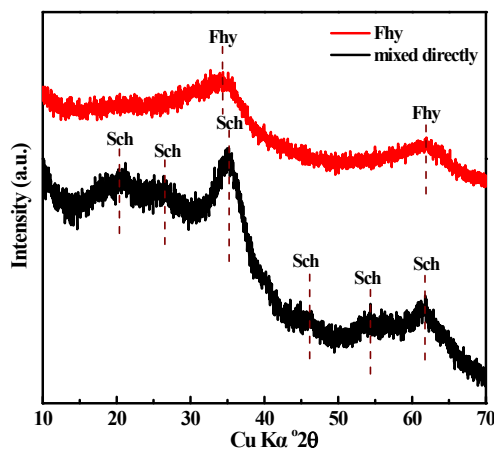


Fig. S2. XRD patterns of the product of “mixed directly” formed through Fe^{3+} hydrolysis

by adding OH^- and of ferrihydrite reference (Sch = schwertmannite, Fhy = Ferrihydrite).

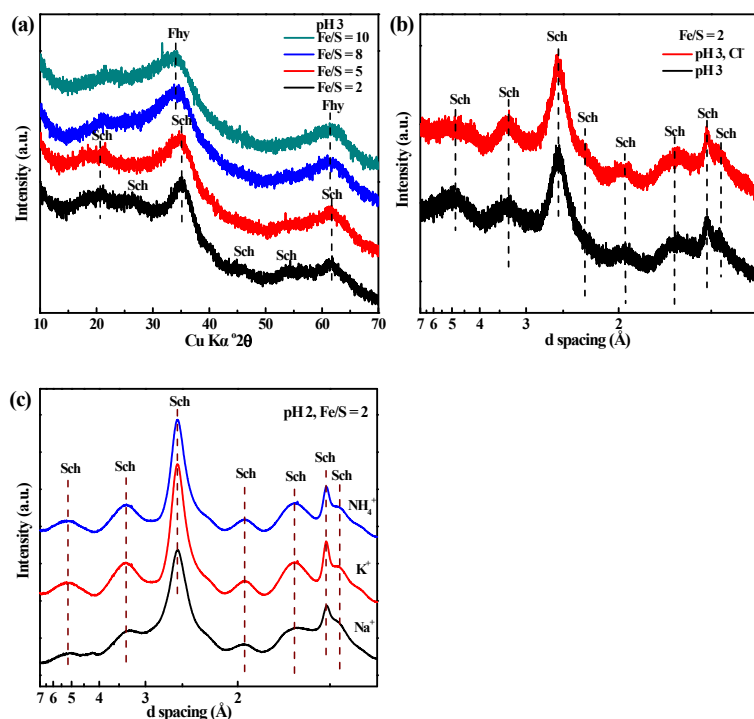
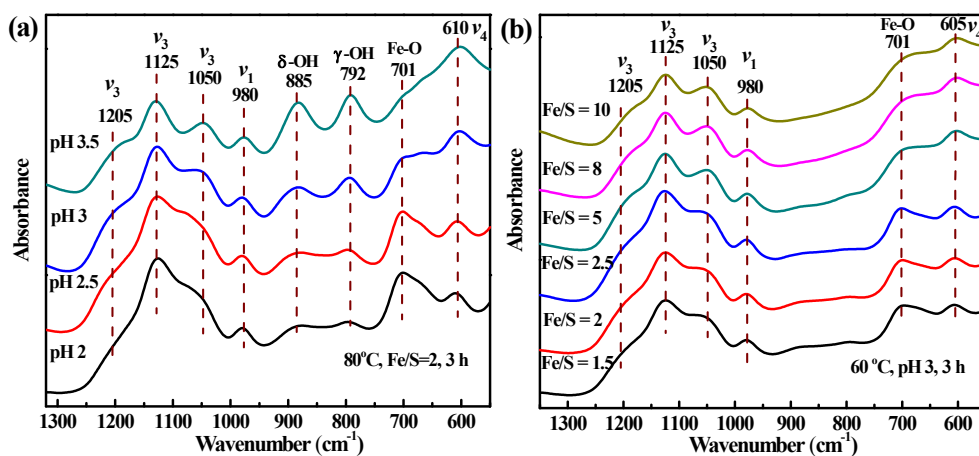


Fig. S3. XRD patterns of the products obtained from Fe^{3+} hydrolysis by adding OH^- over Fe/S molar ratios of 2 – 10 (a), in the presence of Cl^- (b) and K^+ or NH_4^+ (c) (Sch = schwertmannite, Fhy = Ferrihydrite).



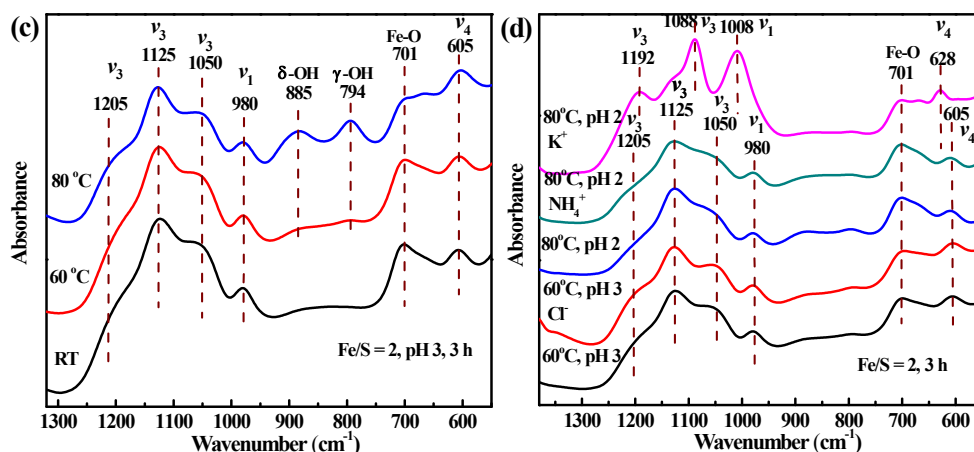


Fig. S4. FTIR spectra of the schwertmannite suspension, obtained from Fe^{3+} hydrolysis by adding OH^- , aged for 3 h at different pHs (a), different Fe/S molar ratios (b), different aging temperatures (c) and in the presence of Cl^- , K^+ or NH_4^+ (d).

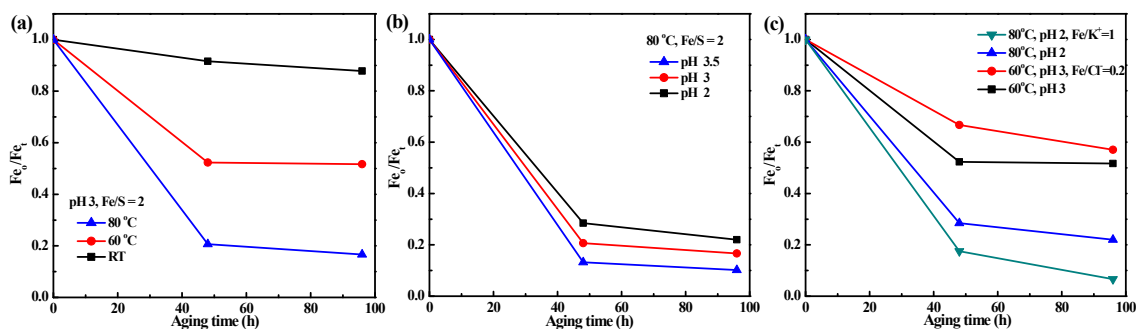


Fig. S5. The transformation rate described as Fe_0/Fe_t of schwertmannite during aging at different temperatures (a), at different pHs (b) and in the presence of Cl^- or K^+ (c) (Fe_0 : weak crystalline iron, dissolved by 0.2 M acidic ammonium oxalate; Fe_t : total iron, dissolved by 4 M HCl).

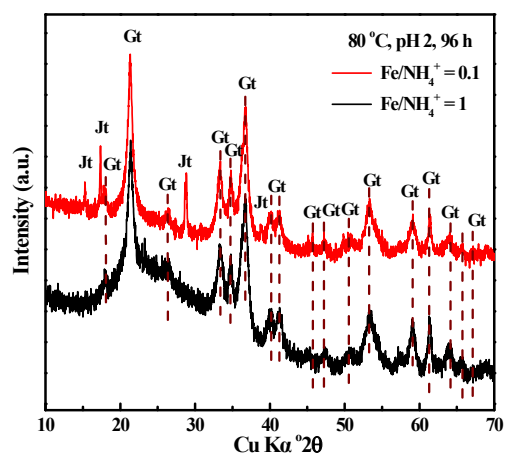


Fig. S6. XRD patterns of the products aged for 96 h in the presence of NH₄⁺ (Fe/NH₄⁺ = 0.1 or 1) at 80 °C and pH 2 (Gt = goethite, Jt = jarosite).